Proceedings of ICFDP 8:
8th International Congress of Fluid Dynamics and Propulsion
December 14-17, 2006, Sharm El-Shiekh, Egypt

ICFDP8-EG-179

TRANSIENT HIGH-SPEED JET FLOW

R. German

Department of Mechanical and Materials Engineering, The University of Western Ontario, London, ON, N6A 5B9, Canada

R.E. Khayat

Department of Mechanical and Materials Engineering, The University of Western Ontario, London, ON, N6A 5B9, Canada

ABSTRACT

The interplay between inertia and gravity is examined in this theoretical study for the steady and transient two-dimensional flow of a thin Newtonian jet film. The fluid emerges from a channel and is driven by both a pressure gradient maintained inside the channel and/or gravity. The flow is dictated by the thin-film equations of the boundary layer type, which are solved by expanding the flow field in terms of orthonormal modes depthwise, and using the Galerkin projection combined with a time-stepping implicit scheme. The strength of inertia relative to gravity is found to be of crucial significance on the film flow.

INTRODUCTION

This study focuses on the influence of inertia and gravity on the steady and unsteady flow of a viscous fluid emerging from a channel (die). Although the modeling and simulation of a liquid laminar jet has been examined previously in the literature, the influence of inertia on transient behavior has not been thoroughly investigated. This is understandable since it is the long-term behavior, after transient effects have died out which is of practical interest. However, when difficulties are encountered in a given film process, the origin of these difficulties may very well lie in the initial stages of the process, long before the process reaches steady state. The problem is of close relevance to a wide variety of industrial processing operations. Details of these processing operations can be found in textbooks on materials processing.[1-2] One of the most important features of the Newtonian jet is that cross-sectional area of the jet changes as the fluid emerges from the channel. The problem consists of obtaining the shape of the free surface and the flow field inside

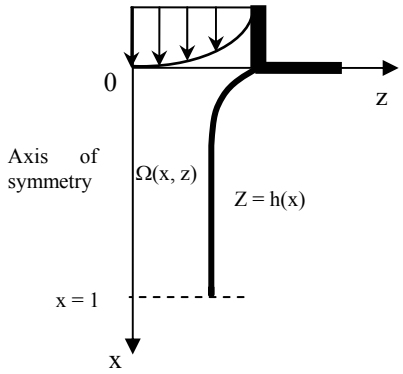

Fig. 1 Schematic illustration of two-dimensional jet flow emerging from a channel. The figure also shows the dimensionless notations used in the formulation.

the domain. The flow is induced by the pressure gradient maintained inside the channel, where fully developed Poiseuille conditions are assumed to prevail. Given the small thickness of the fluid jet compared to jet length and local curvature, the thin-film approximation will be used.

Several theoretical analyses of the steady-state Newtonian jet flow have been presented in the literature. Neglecting viscous forces, Harmon[3] obtained for the circular jet the asymptotic contraction ratio (a ratio between a radius downstream where the profile has flattened and the radius at the tube exit) $\sqrt{3}/2$ by considering the balance of mass transport and momentum along the jet, taking plug flow at infinity and parabolic profile at the exit. The analogue ratio for the two-dimensional jet, $5/6$, was obtained by Tillett,[4] who used the method of matched asymptotic expansions. The

method, however, gives accurate results only for moderate distances downstream. Addachi[5] studied the problem for a viscous gravity jet as well as inertia gravity jet falling vertically in the atmosphere, for which he obtained an analytical solution however with the assumption of flat profiles of velocity and pressure over its horizontal cross-section. Harmon's result was experimentally confirmed by Goren and Wronski[6] for high Reynolds number, though still in laminar flow regime. Their measurements show that the radius of the jet expands or contracts depending on the Reynolds number. To sum up, there is no quantitative analytical theory of the dynamics of the fluid emerging from a channel.[7] However, there are numerous studies devoted to the numerical solution of the steady jet flow, involving various degrees of approximation. First successful solution is due to Nickel et al.,[8] who solved the problem of a creeping Newtonian circular jet by finite element method. The solution shows that at the point of exit where there is a sudden change in boundary condition there is a stress singularity. The method was further extended for higher Reynolds number by Reddy and Tanner,[9] and for surface tension effects by Omodei[10]. Concerning Newtonian fluids, the value of the contraction/expansion ratio was found by most of the researchers to be approximately 1.12-1.13 for creeping flow,[11] which is in good agreement with experimental results.[6, 12]

Generally, studies on thin-film flow involve either gravity- or surface-tension-driven flow.[13,14] The flow of a falling film on an inclined or vertical wall is particularly emphasized in the literature.[13] The interplay between inertia and other forces in thin-film flow has been less examined in the literature.[15-20] Attempts have been made to extend the classical Reynolds equation to include the effect of fluid inertia in thin-film theory.[18] More recently, Khayat and co-workers examined the influence of inertia in the film flow of Newtonian[21-23] and non-Newtonian[24,25] fluids. Watson[17] examined much earlier the steady laminar and turbulent radial spreading of a liquid jet over a horizontal plane, including the special case of two-dimensional flow. For a large distance from the source, a similarity solution of the laminar boundary-layer equation was sought. In particular, Watson found that for two-dimensional flow, the steady (dimensionless) shape of the free surface is given by $h_s = \pi x/\sqrt{3}\,\mathrm{Re} = 1.81x/\mathrm{Re}$, where x is the distance from the source, and Re is the (modified) Reynolds number.[26] The steady surface profile was obtained in the absence of gravity and surface tension. It constitutes an important limit form against which nonlinear film flow formulations may be validated.

Although the thin-film formulation reduces the pressure to its hydrostatic part, thus eliminating the momentum equation in the depthwise direction from the problem, the dimension of the problem remains the same as originally. Benney's long wave (LW) approximation is often used,[27] especially for small inertia flow. At high Reynolds number, inertia is better accounted for through the "boundary layer" (BL) approximation, which includes the effect of depthwise flow. A finite-element solution of the full Navier-Stokes equations for the flow in a falling film was carried out by Salamon et al.[28] Comparison of the finite-element and LW results indicates that serious limitations exist in the validity of the LW equation. The major difference between the original Navier-Stokes and BL equations is the hydrostatic variation of the pressure across the film depth. As a result, only the depthwise momentum equation is eliminated, but the convective terms are retained in the remaining equations, and the number of boundary conditions is reduced. However, the solution of the BL equations remains essentially as difficult to obtain as that of the Navier-Stokes equation.[20] A depthwise integration of the momentum equation(s) in the lateral direction(s) is usually performed by assuming a self-similar semi-parabolic flow profile in the depthwise direction, as was proposed by Shkadov.[29] Although the depth-averaged equations are only of second order in time, they yield plausible results, at least qualitatively, but they remain fundamentally questionable because of the semi-parabolic profile assumption.[20] A measure of the error involved may be inferred by computing the free-surface profile (dimensionless) in the absence of gravity and surface tension, and comparing it to the Watson's result given above. From the literature, the steady-state profile based on the semi-parabolic profile is easily found to be $h_S = 2.5x/\mathrm{Re}$.[13] The parabolic approximation is widely used in the literature, and its validity was established experimentally.[15] However, it is generally argued that the parabolic approximation is valid at low or moderately low Reynolds number, and provided that the waves are far from the entry.[30] In addition to high-inertia flow, other flow conditions that restrict the range of validity of the semi-parabolic profile include the presence of end effect, turbulent flow, and (most likely) nonlinear effects stemming from shear-thinning or viscoelastic effects.[24,25] Ryuer-Quill et al.[31] used a three-term expansion of the flow in the depthwise direction to obtain three coupled equations for free surface height, flow rate and stress. Takeshi examined the flow in a falling film at moderate Reynolds number and large but finite Weber number, using a regularization method, which consists of a combination of the Pade approximation and long-wave expansion.[20]

In this study, a unified spectral approach is proposed to model the pressure/gravity-driven flow of a Newtonian thin-film jet. Given the importance of inertia, the BL formulation rather than Benney's LW approximation will be used. Surface tension is not considered. In the jet problem, surface tension tends to bring the jet shape to a uniform thickness profile commensurate with the channel height. Even though the surface tension effect is considerably strong for low inertia flow, it decreases rapidly with increase of inertia. Omodei[10] in his work reports that for example at Re = 1 the height of the free surface changes by 8% when surface tension parameter, S ($S = \sigma\rho H/\mu^2$, where σ is the surface tension coefficient), changes from 0 to 1.2. However, for $\mathrm{Re} \geq 10$ the height of the free surface changes by less than 1% for $S \in [0, 12]$. Although the height of the jet surface depends on the surface tension, to see this dependence for larger Re one would have to use much

larger S than 12. The value of S in experiments on capillary jets carried out by Goren and Wronski[6] ranged from 0.054 to 9.4. The situation is different in the case of transient analysis. As it was shown by Lee and Mei,[32] small amount of surface tension will qualitatively change the response of a flow and therefore our solution should be considered as valid only for flow with negligible surface tension effect. The flow equations are first mapped onto the rectangular domain, and a formal expansion of the velocity field is introduced in terms of orthonormal basis functions. The formulation is similar to the one used previously,[21-25] which gave excellent agreement with Watson's similarity solution for liquid spreading. The method follows closely and generalizes the formulation of Zienkiewicz and Heinrich,[33] which emphasizes water flow over extended areas. There are, however, two major simplifying assumptions adopted by Zienkiewicz and Heinrich,[33] which will be relaxed in the present study. First, the depthwise velocity component and its derivative will not be neglected in the momentum equation. Second, despite the long-wave approximation, the spatio-temporal variation in surface height will not be neglected in the momentum equation. The Galerkin projection method is used to generate the equations that govern the expansion coefficients. The spectral method, and, particularly, the low-dimensional description of flow, has emerged as an effective alternative to conventional methods.[34] Although this method has predominantly been used for simple flow, recent developments have included complex geometry,[35] and complex fluids.[36-38] Unlike the depth-averaging method, the proposed spectral methodology becomes particularly suited for highly nonlinear thin-film flow. Details of the free surface and flow field can be captured explicitly as well as in the mean sense.

PROBLEM FORMULATION AND SOLUTION PROCEDURE

The general thin-film formulation is implemented for a jet. The equations and boundary conditions are deduced for a flow driven by an imposed pressure gradient at the exit of the channel. The solution of the resulting BL equations is then discussed.

Thin-film equations and boundary conditions

Consider the two-dimensional flow of an incompressible Newtonian fluid of density ρ and viscosity μ. In this work, inertia effect is assumed to be dominant and surface tension effect is neglected. The flow is induced by a pressure gradient inside the channel (Poiseuille flow) of width H upstream, and by the action of gravity. In this case, L and H will be taken as the reference length and thickness in the streamwise and depthwise directions, respectively, with x and z being the corresponding dimensionless coordinates. Here L is the length of the jet. The streamwise and depthwise velocity components are scaled by V and HV/L, respectively, where V is a reference velocity, which is taken as the maximum velocity inside the channel. The pressure is scaled by $\mu VL/H^2$. The scaling for pressure is chosen to ensure the balance between pressure and viscous forces.[24] Figure 1 illustrates schematically the problem in the (x, z) plane. The (dimensionless) shape of the free surface is given by z = h(x, t), which is scaled by H. The fluid is assumed to occupy the domain $\Omega(x, z)$, which is bounded by the channel exit (x = 0), the axis of symmetry (z = 0), the free surface, z = h(x, t), and the end x = 1. There are three important dimensionless groups that emerge, namely, the Reynolds number, Re, the Froude number, Fr, and the aspect ratio, ε:

$$\mathrm{Re} = \frac{\rho V H^2}{L\mu}, \quad \mathrm{Fr} = \frac{V}{\sqrt{gL}}, \quad \varepsilon = \frac{H}{L}, \tag{1}$$

where g is the gravitational acceleration in the x direction. The conservation equations are obtained in dimensionless form, with terms of $O(\varepsilon^2)$ and higher being excluded. In this case, the momentum equation in the depthwise direction simply states that the pressure is reduced to its hydrostatic part. It is also assumed that no external (wind) pressure acts on the free surface. In the current formulation, the conservation equations reduce to:

$$u_{,x} + w_{,z} = 0, \tag{2}$$

$$\mathrm{Re}\left(u_{,t} + uu_{,x} + wu_{,z}\right) = \frac{\mathrm{Re}}{\mathrm{Fr}^2} + u_{,zz}, \tag{3}$$

where u(x, z, t) and w(x, z, t) are the streamwise and depthwise velocity components, respectively. Here a subscript after a comma denotes partial differentiation. Re is sometimes referred to as the modified Reynolds number in boundary-layer or lubrication theory.[26] Equation (3) was obtained upon combining the momentum equations in the streamwise (x) and depthwise (z) directions.

The shape of the free surface is dictated by the kinematic condition:

$$h_{,t} + u(x, z = h, t)h_{,x} = w(x, z = h, t). \tag{4}$$

The relevant dynamic condition reads

$$u_{,z}(x, z = h, t) = 0. \tag{5}$$

Note that another dynamic condition is the vanishing of the pressure at the film surface. In this case, the pressure vanishes everywhere. The conditions of symmetry give:

$$u_{,z}(x, z = 0, t) = w(x, z = 0, t) = 0. \tag{6}$$

Flow conditions at the channel (die) exit are assumed to be known. Since Poiseuille flow holds at the channel exit, then

$$u(x = 0,z, t) = 1 - z^2, \quad h(x = 0,t) = 1. \tag{7}$$

Equation (3) is of the "boundary layer" type, which must be solved subject to conditions (6)-(7) in the z direction, as well as appropriate initial conditions to be specified later.

Solution procedure

Given the small thickness of the film, the governing equations are customarily depth-averaged across the thickness. This step is justified on the basis that the flow field should not vary significantly in the z direction. However, the presence of the nonlinear convective terms in equation (3) prohibits the conduction of an exact averaging process. The key difficulty, of course, is the explicit z dependence of the velocity components. Even if the x and z dependencies are assumed to be decoupled, with a separation of variable type argument becoming possible, the question remains as to the type of z dependence that u and w must have. Several types and levels of approximations have been used in the literature, the most prominent of which being the assumption of a similarity semi-parabolic profile.[13] Expectedly, the similarity profile loses its validity when inertia becomes important. In this case, more formal treatments in the form of flow expansion in the z direction were suggested.[20-25]

In this paper, equation (3) is further reduced by expanding the flow field in terms of appropriately chosen orthonormal modes in the z direction, and applying the Galerkin projection method to generate the equations that govern the expansion coefficients. The procedure includes the depth averaging technique as a limit case. The first step involves the mapping of the physical domain onto a straight strip. The following transformation is introduced, namely

$$\chi(x,z,t) = x, \quad \xi(x,z,t) = \frac{z}{h(x,t)}, \quad \tau(x,z,t) = t. \tag{8}$$

Thus, the physical domain [0,1] × [0, h(x, t)] is mapped onto [0,1] × [0,1]. The governing equations become

$$hu_{,\chi} - h_{,\chi}\xi u_{,\xi} + w_{,\xi} = 0, \tag{9}$$

$$\mathrm{Re}\, h\left[hu_{,\tau} - \xi u_{,\xi} h_{,\tau} + u\left(hu_{,\chi} - h_{,\chi}\xi u_{,\xi}\right) + wu_{,\xi}\right] = \frac{\mathrm{Re}}{\mathrm{Fr}^2} h^2 + u_{,\xi\xi}. \tag{10}$$

The streamwise velocity component u is represented in terms of orthonormal basis functions, $\Phi_i(\xi)$, such that

$$u(\chi,\xi,\tau) = \sum_{i=1}^{M} U_i(\chi,\tau)\Phi_i(\xi), \tag{11}$$

where M is the number of modes, and $U_i(\chi, \tau)$ are the unknown expansion coefficients. The shape functions are taken to satisfy conditions (5) and (6) as well as orthonormality. Thus,

$$\left\langle \Phi_i \Phi_j \right\rangle = \delta_{ij}, \quad \Phi_{i,\xi}(\xi = 0) = \Phi_{i,\xi}(\xi = 1) = 0, \quad \forall i, j \in [1, M], \tag{12}$$

where δ_{ij} is the Kronecker delta, and $\langle\ \rangle$ denotes the integral over $\xi \in [0, 1]$. In this work, the shape functions are taken to be simple polynomials, of order zero, 3, 4, 5 and so on. Other shape functions are of course possible, and have been examined in previous studies. It is generally found that for thin-film flow the number of modes is low, and the choice of the shape functions is not critical.[21-25] It will be argued that any arbitrary number of modes can be introduced, each satisfying conditions (12), but reasonable depthwise distributions can be obtained with M = 2 or M = 3 for most practical applications.[23] More importantly, higher-order modes seem to lead only to a slightly better accuracy, without changing the qualitative picture. These observations will be confirmed below when convergence and accuracy are assessed. Of course, the rate of convergence will strongly depend on the choice of the modes. In addition, given the small thickness of the fluid film, the flow field is not expected to vary strongly with the height z.

The depthwise velocity component is obtained by substituting (11) into equation (9) and integrating the latter over the interval [0, ξ], to give

$$w(\chi,\xi,\tau) = \sum_{i=1}^{M}\left[h_{,\chi}\left(\xi\Phi_i - \varphi_i\right)U_i - h\varphi_i U_{i,\chi}\right], \tag{13}$$

where $\varphi_i(\xi) = \int_0^{\xi} \Phi_i d\xi$. Upon use of expressions (11) and (13), the kinematic condition (4) becomes

$$h_{,\chi} = -\frac{h\sum_{i=1}^{M} U_{i,\chi}\langle\Phi_i\rangle + h_{,\tau}}{\sum_{i=1}^{M} U_i\langle\Phi_i\rangle}. \tag{14}$$

A hierarchy of equations is obtained for the coefficients $U_i(\chi,\tau)$, when expressions (11), (13) and (14) are substituted into the momentum equation (10), which is then multiplied by $\Phi_{i\geq 1}$ and integrated over $\xi \in [0, 1]$. Thus, one has

$$\sum_{p=1}^{M}\langle\Phi_i\Phi_p\rangle U_{p,\tau}+\sum_{j=1}^{M}\left[\sum_{k=1}^{M}\left(\left\langle\Phi_i\left(\Phi_j\Phi_k-\varphi_k\Phi_{j,\xi}\right)\right\rangle+\frac{\langle\Phi_k\rangle}{\sum_{m=1}^{M}\langle\Phi_m\rangle U_m}\sum_{r=1}^{M}\langle\Phi_i\varphi_j\Phi_{r,\xi}\rangle U_r\right)U_{k,\chi}\right.$$
$$\left.+\frac{h_{,\tau}}{h}\left(\frac{\sum_{r=1}^{M}\langle\Phi_i\varphi_j\Phi_{r,\xi}\rangle U_r}{\sum_{m=1}^{M}\langle\Phi_m\rangle U_m}-\langle\xi\Phi_i\Phi_{j,\xi}\rangle\right)\right]U_j$$
$$=\frac{\langle\Phi_i\rangle}{Fr^2}+\frac{1}{h^2\,Re}\sum_{j=1}^{M}\langle\Phi_i\Phi_{j,\xi\xi}\rangle U_j \qquad (15)$$

Equations (14) and (15) reflect a system of nonlinear partial differential equations with M +1 degrees of freedom. The boundary conditions are deduced from (7) and (11), leading to

$$h(\chi=0,\tau)=1,$$
$$U_i(\chi=0,\tau)=\left\langle\left(1-\xi^2\right)\Phi_i\right\rangle. \qquad (16)$$

The initial conditions must also satisfy conditions (16), and may generally be written as

$$h(\chi,\,\tau=0)=f(\chi),$$
$$U_i(\chi,\,\tau=0)=\left\langle\left(1-\xi^2\right)\Phi_i\right\rangle g(\chi), \qquad (17)$$

where f and g are to be specified. The fluid occupies the domain $x \in [0, 1]$ at all times. First, it is assumed that the film has a constant height. Later, the initial height is assumed to exponentially decrease, and finally, steady state profiles of height are used. The solution of the system (14) - (15), subject to conditions (16) - (17), is solved by using an implicit forward finite-difference method in time, combined with sixth-order Runge-Kutta integration in the streamwise direction.

DISCUSSION AND RESULTS

The formulation and numerical implementation above are now applied to the jet flow schematically illustrated in Fig. 1. The influence of inertia and gravity are explored both for steady and transient flows. The numerical accuracy is assessed and the convergence of the method is examining. Some limit cases are also discussed.

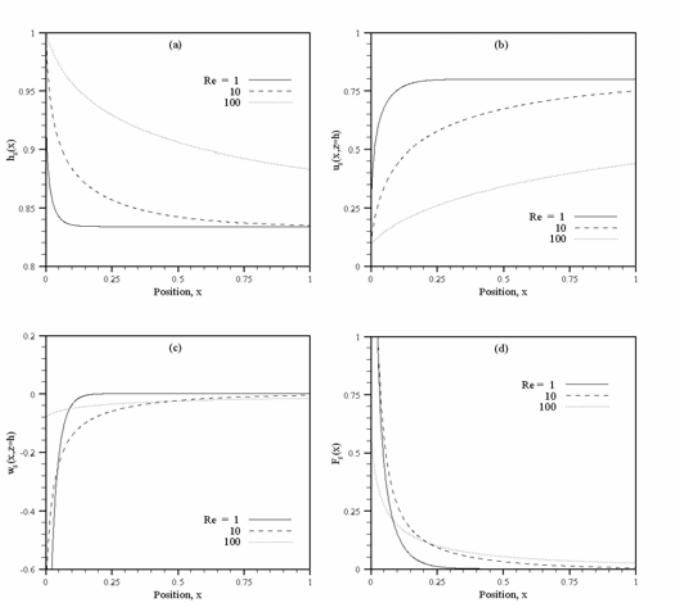

Fig. 2 Influence of inertia on the steady-state laminar jet flow for $Re \in [1, 100]$ in the absence of gravity ($Fr\to\infty$). Distribution of (a) jet thickness, $h_s(x)$, (b) streamwise velocity component, $u_s(x, z = h)$, (c) depthwise velocity component at the jet surface, $w_s(x, z = h)$, and (d) axial traction, $F_s(x)$.

Steady-state flow

The influence of inertia on steady flow is examined by varying the Reynolds number over the range $Re \in [1,100]$ while gravity is assumed to be negligible at first ($Fr \to \infty$). The flow response is illustrated in Fig. 2, where the steady film thickness, $h_s(x)$, streamwise velocity, $u_s(x, z = h)$, the depthwise velocity, $w_s(x, z = h)$, at the free surface, and the axial force, $F_s(x)$, are plotted against x for various Re values. The behavior of the thickness is basically opposite to that of the streamwise flow. It must be noted, however, that h_s is not simply inversely proportional to u_s, as the case would have been for an elongation-dominated flow (such as in film casting). While h_s decreases, u_s increases with x, at any Reynolds number. The behavior appears to be always monotonic. At low Reynolds number, the jump in streamwise velocity and drop in film thickness are accompanied by a jump in the depthwise velocity and axial force near x = 0. The depthwise flow and axial force diminish with x, and eventually asymptotically vanish for any Re. In fact, since the pressure is essentially atmospheric throughout the film, the axial force is reduced to axial extensional rate, calculated at z = 0. The figure suggests a depthwise flow movement towards the jet core, resulting in film contraction. Simultaneously, the film thickness tends to a

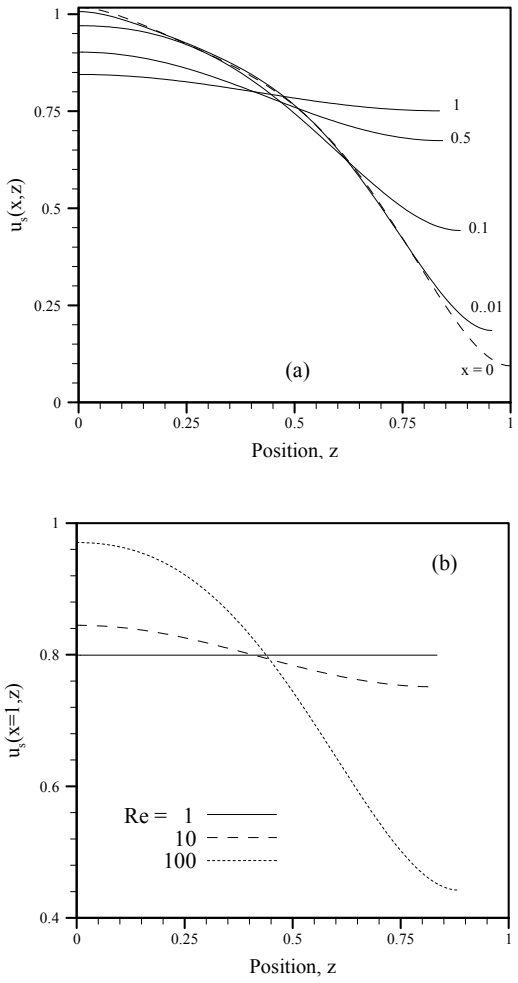

Fig. 3 Streamwise velocity distribution, (a) at various distance x from the channel exit for Re = 10, (b) at x = 1 for Re = 1, 10, and 100. Gravity is neglected.

constant value, where plug-flow conditions prevail. The depthwise flow near the channel exit becomes stronger with diminishing inertia. Similarly, the jump in u_s and drop in h_s are sharper for smaller Re. In fact, the flow becomes singular in the limit of creeping flow.

Streamwise velocity profiles at various locations are depicted in Fig. 3a for Re = 10. The influence of inertia on the velocity profile at x = 1 is depicted from Fig. 3b. In general, for low-inertia flow, the velocity becomes essentially uniform (plug flow) within a short distance from the channel exit. In this case, the parabolic profile at the channel exit is quickly damped out by viscous effect, resulting in a solid-plug movement. For high-inertia flow the parabolic velocity profile persists throughout the jet region, reflecting the presence of similarity flow. For moderate-inertia flow, the situation is typically illustrated in Fig. 3a, where plug-flow conditions set in for x > 0.5. Further insight is gained upon examining the

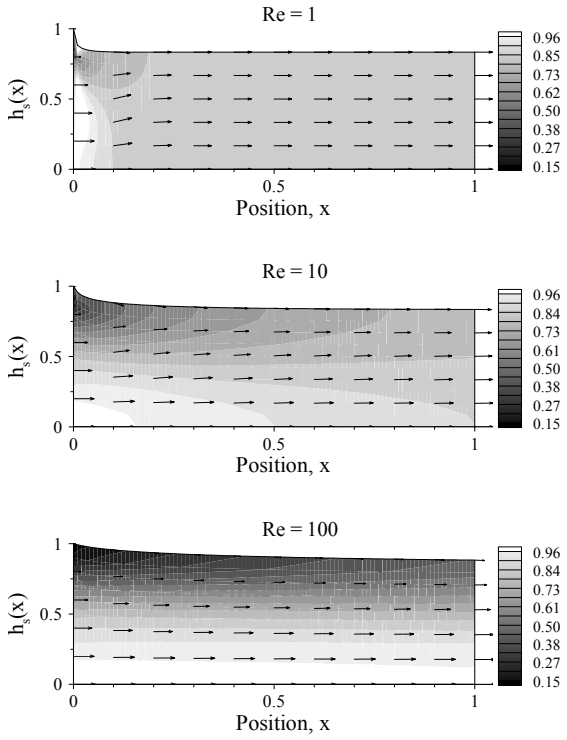

Fig. 4 Steady-state flow field and contours of velocity magnitudes at Re = 1, 10, and 100 in the absence of gravity (Fr $\rightarrow \infty$).

flow field. Figure 4 displays the flow direction and contours of velocity magnitude for Re = 1, 10 and 100. The flow towards the free surface is particularly obvious for Re = 1, despite the relatively strong contraction of the film at the channel exit.

Thus, near the exit, contraction near the free surface is opposed by an expansion in the jet core. Note also the sharp transition towards plug-flow conditions, which essentially sets in everywhere for x > 0.4. Elongational flow is clearly dominant in this case. In contrast, at higher Re, although the flow becomes predominant in the streamwise direction, the velocity magnitude tends to change rapidly with both x and z. For Re = 10, both shear and elongational effects appear to be present. At even higher Re, the flow begins to homogenize in layers, with a plug-flow emerging in the core region only. Shearing is clearly dominant in this case.

The effect of gravity is examined by varying Fr. Gravity is found to have a dramatic effect on the film shape and flow. In this case, Re is set equal to a moderately small value, namely, 10. The film profiles and flow response are depicted in Fig. 5. It is observed that as the influence of gravity increases, the film contracts further, more than 50% for Fr = 1. Simultaneously, the increase in $u_s(x, z = h)$ becomes more significant, thus delaying the transition to plug flow (downstream). Similarly to the decrease in film thickness, the depthwise velocity, w_s, decreases as Fr decreases. Overall, the depthwise flow gains considerable strength with gravity,

especially near the channel exit where film contraction occurs. This is also confirmed from the force distributions, which

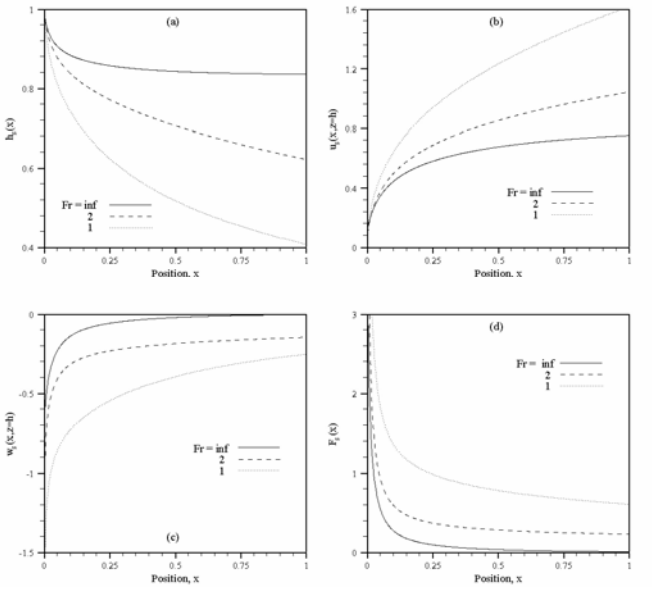

Fig. 5 Influence of gravity on the steady-state jet flow, for $Fr \in [1, \infty)$ and $Re = 10$. Distribution of (a) jet thickness, $h_s(x)$, (b) streamwise velocity component, $u_s(x, z = h)$, (c) depthwise velocity component at the jet surface, $w_s(x, z = h)$, and (d) axial traction, $F_s(x)$.

clearly show the increase of elongation due to gravity. In sum, gravity effect is similar to inertia as it enhances elongational flow.

Convergence of the method is assessed by examining the influence of number of modes M. It is generally found that only a few modes are needed to secure an acceptable rate of convergence. This observation has been consistently made for other film flows, such as the coating by Newtonian[21,23] and non-Newtonian[24,25] films of a rigid substrate of arbitrary shape. Different types of orthonormal functions have been used including trigonometric and Chandrasekhar functions.[21] Polynomial functions, such as the ones used here, are found to yield a high level of convergence and accuracy, and are simultaneously easy to implement. The influence of the number of modes is typically illustrated in Fig. 6 for a flow with $Fr = 1$ and $Re = 10$. The figure displays the distributions of U_1, U_2, U_3 and U_4 with respect to x. The two leading modes, U_1 and U_2 are clearly dominant at any position, with U_3 being almost one order of magnitude smaller, and U_4 being essentially negligible. The fast rate of convergence is also confirmed for $h_s(x)$ and $u_s(x, z = h)$, as shown in Figs. 6b and 6c, respectively. This was confirmed through calculations carried out at different inertia levels and in presence or absence of gravity (not shown).

While convergence can be assessed by varying the grid size and number of modes in the solution expansion, the accuracy needs to be determined by comparison against existing

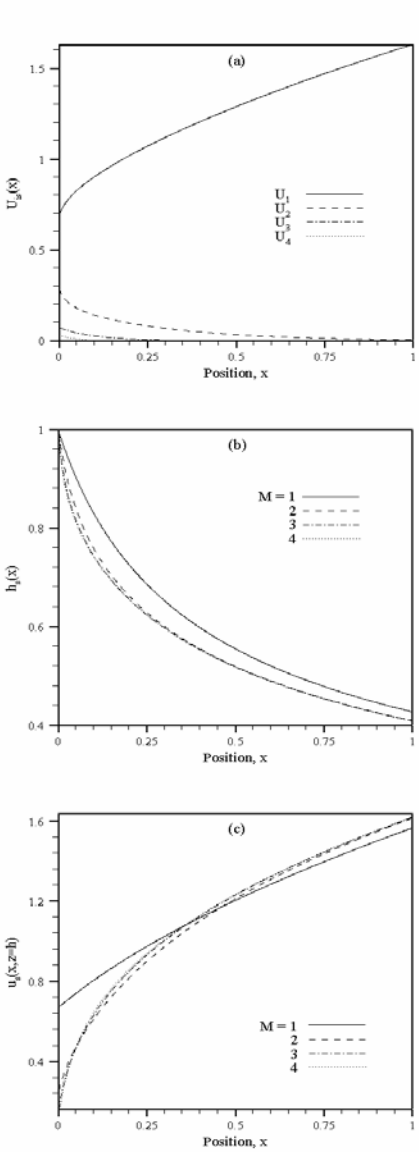

Fig. 6 Mode distribution for $M = 4$ and influence of higher-order modes for $Re = 10$ and $Fr = 1$. Shown are distributions of: (a) expansion coefficients $U_{is}(x)$, (b) jet thickness $h_s(x)$, and (c) streamwise velocity $u_s(x, z=h)$, for $1 \le i \le 4$.

formulations and limit cases. For coating flow, a useful limit flow was considered previously for comparison, namely, Watson's similarity solution for the spreading of a liquid film on a rigid surface at moderately high Reynolds number.[20] Excellent agreement was reached using a spectral expansion and the boundary-layer equations, similarly to the current formulation.[28] Comparison with other formulations, mainly the depth-averaging procedure, leads to poor agreement.[16] A similar level of accuracy is expected in the present problem given the similarity of the procedure used in coating flow. In the present case, limit flows are obtained by taking extreme

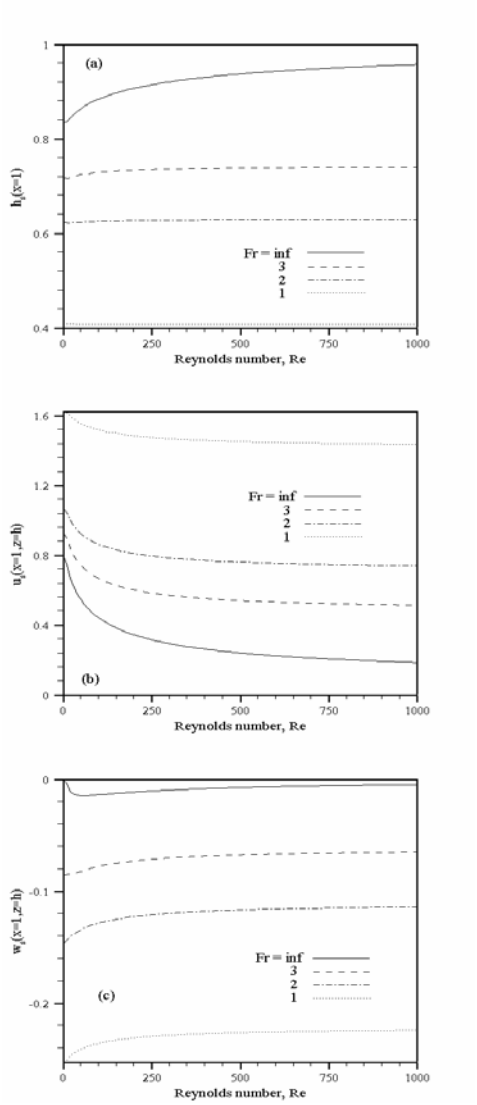

Fig. 7 Interplay between inertia and gravity. The figure shows: (a) thickness, (b) streamwise velocity, and (c) depthwise velocity distribution of the steady-state jet flow at the distance x = 1, as a function of Reynolds number for Fr $\rightarrow \infty$, Fr = 3, 2, and 1.

values of the Reynolds and Froude numbers, thus simplifying the problem and the solution procedure, on the one hand, and allowing comparison with and validation of the general solution procedure above, on the other hand. These limit flows will be considered once the overall influence of inertia and gravity is examined next.

The overall influence of both inertia and gravity is now assessed by examining the flow response at x = 1. The results are shown in Fig. 7 where the film thickness, and velocity components are plotted against Re for Fr = 1, 2, 3 and ∞. In general, the film thickness increases, and the streamwise velocity decreases monotonically with Re. In the absence of gravity, the depthwise flow is negligible when Re is very small. This is in accordance with the creeping flow limit discussed earlier. As Re increases,

however, $w_s(x = 1, z = h)$ exhibits a minimum at Re $\approx$ 50 and asymptotically approaches zero as Re increases further. In the presence of gravity, the thickness distribution becomes almost independent of Re, whereas the streamwise velocity still decreases rather strongly near the creeping limit, but eventually levels off for large Re. The minimum in the depthwise velocity occurs at a smaller Reynolds number as the effect of gravity increases, and eventually disappears for Fr > 3.

Consider now the limit of a flow with dominant inertia and negligible gravity. For steady-state flow, the governing equations reduce to

$$u_{,x} + w_{,z} = 0, \quad uu_{,x} + wu_{,z} = 0, \qquad u(x, z = h)h_{,x} = w(x, z = h). \tag{18}$$

In this case, the equations and boundary conditions are satisfied by the solution

$$u_s(x, z) = 1 - z^2, \quad w_s(x, z) = 0, \quad h_s(x) = 1, \tag{19}$$

which reflects a similarity flow throughout the jet. The validity of the current formulation is assessed against the limit solution (19) for large Re. In the large Re limit, Fig. 7 confirms that the film

recovers the conditions at the channel exit, namely a thickness value equal to one, and vanishing velocity at the free surface (z = 1), in agreement with expressions (19). The results of Fig. 7 are further verified for x $\in$ [0, 1].

Consider next the limit of creeping flow (Re $\rightarrow$ 0). It is important to realize that the problem becomes singular in this limit, as indicated by equation (3). Indeed, if Re is set equal to zero, then convective terms such as uu_x, or more precisely u_x, need to be set to infinity for u to remain finite, say near the channel exit. This means, in reality, that the flow undergoes a significant elongation at small Reynolds number. The singular flow response at the exit of the channel is clearly evident from Fig. 2 for Reynolds number one.

Transient jet flow

The interplay between inertia and gravity will now be explored under transient conditions. The transient flow response depends strongly on the type of initial conditions used. In the results reported below, the initial conditions are shown in dashed lines, and the steady-state curves are included for reference. Consider first the influence of inertia on transient behavior for a flow subject to flat initial conditions. In this case,

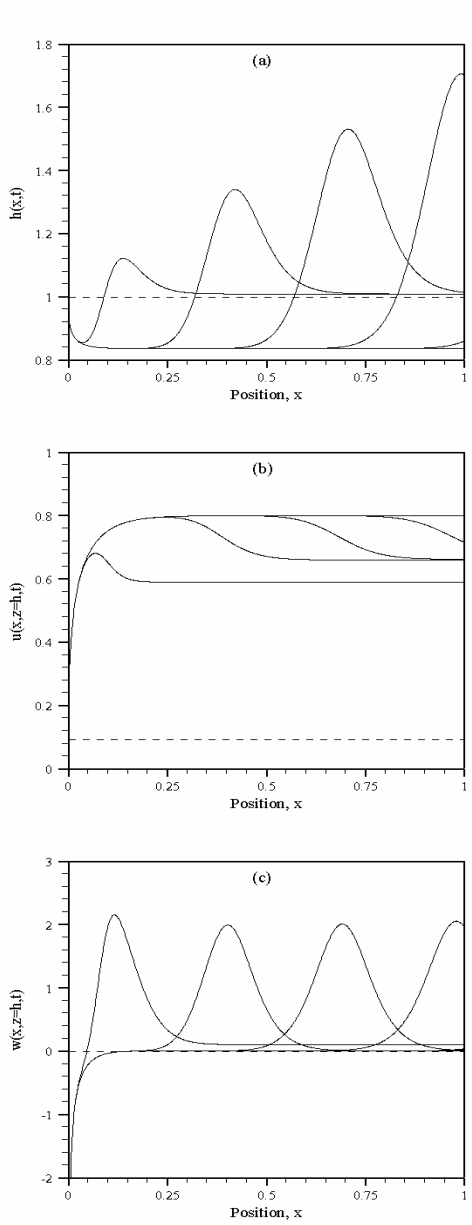

Fig. 8 Evolution of free surface (a), streamwise velocity component at the free surface (b), and depthwise velocity component at the free surface (c), for Newtonian jet flow. Re = 1 and $\mathrm{Fr} \to \infty$ at constant intervals 0.2, including initial profiles (dashed line).

$$f(x) = g(x) = 1 . \tag{20}$$

Gravity effect is assumed to be negligible at first ($\mathrm{Fr} \to \infty$). The flow response is shown in Fig. 8 for low Reynolds number, Re = 1. Initially, the flow experiences a sudden jump (from flat conditions), which is mostly felt near the channel exit. Figure 8a shows the film thickness, h(x, t) at equal intervals of time for a period of 1 time unit. In the early stages, the film thickness exhibits a contraction near the channel exit, with the film reaching already the steady state near x = 0. The contraction, however, coincides with the occurrence of a minimum at some x > 0. The film height rises further downstream, exhibiting a maximum (forming a sine wave), and asymptotically embracing the initial height for large x. With time, the disturbance propagates downstream with increase in amplitude. It is important to note that there is no significant steepening in the wave; this behavior is typical for the type of initial conditions used and will be investigated later. After some time, t ≈ 1, the steady-state conditions are reached over the whole computational domain. The corresponding streamwise

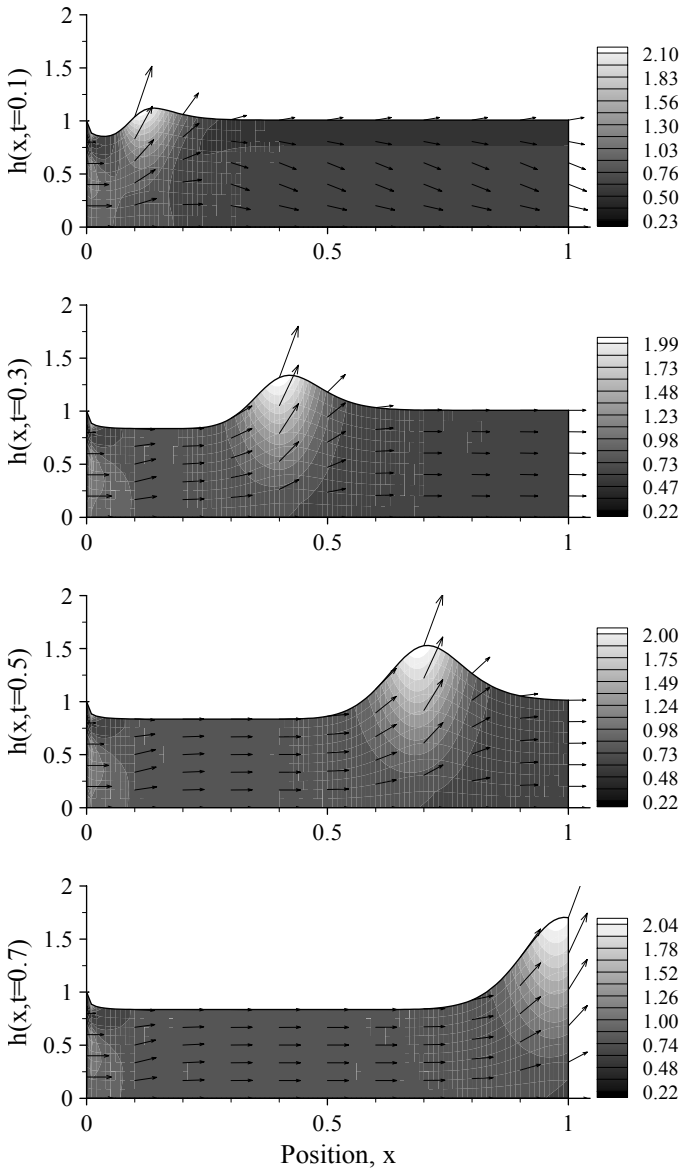

Fig. 9 Evolution of flow field and contours of velocity magnitude for low-inertia flow, Re = 1, in the absence of gravity. The figure shows the flow fields at constant intervals 0.2 over a period of 0.7 time units.

E

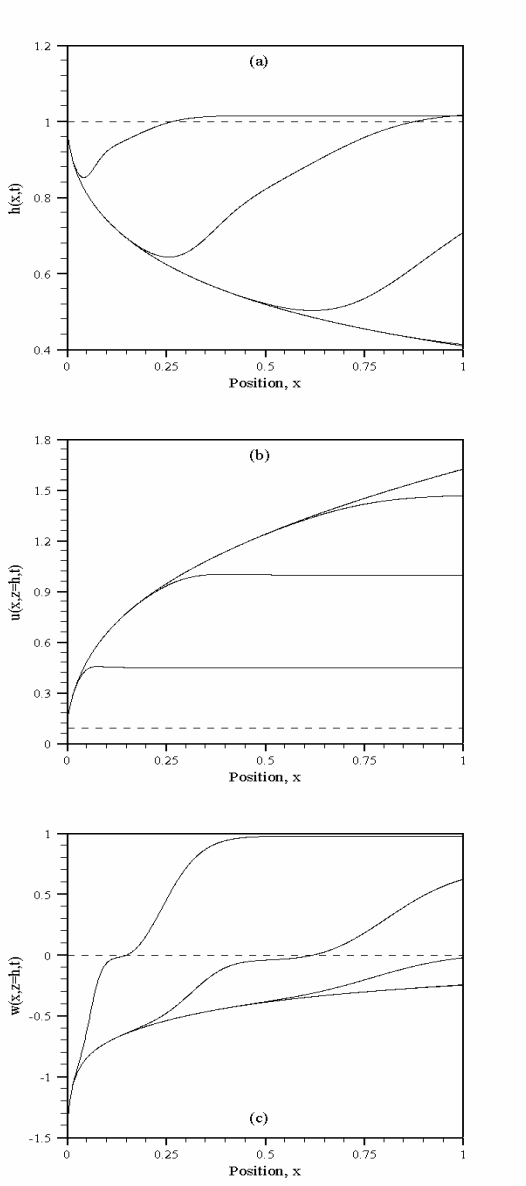

Fig. 12 Evolution of free surface (a), streamwise velocity component at the free surface (b), and depthwise velocity component at the free surface (c), for moderately low-inertia flow, Re = 10, in the presence of strong influence of gravity, Fr = 1, at constant intervals 0.2. Initial profiles are also included (dashed line).

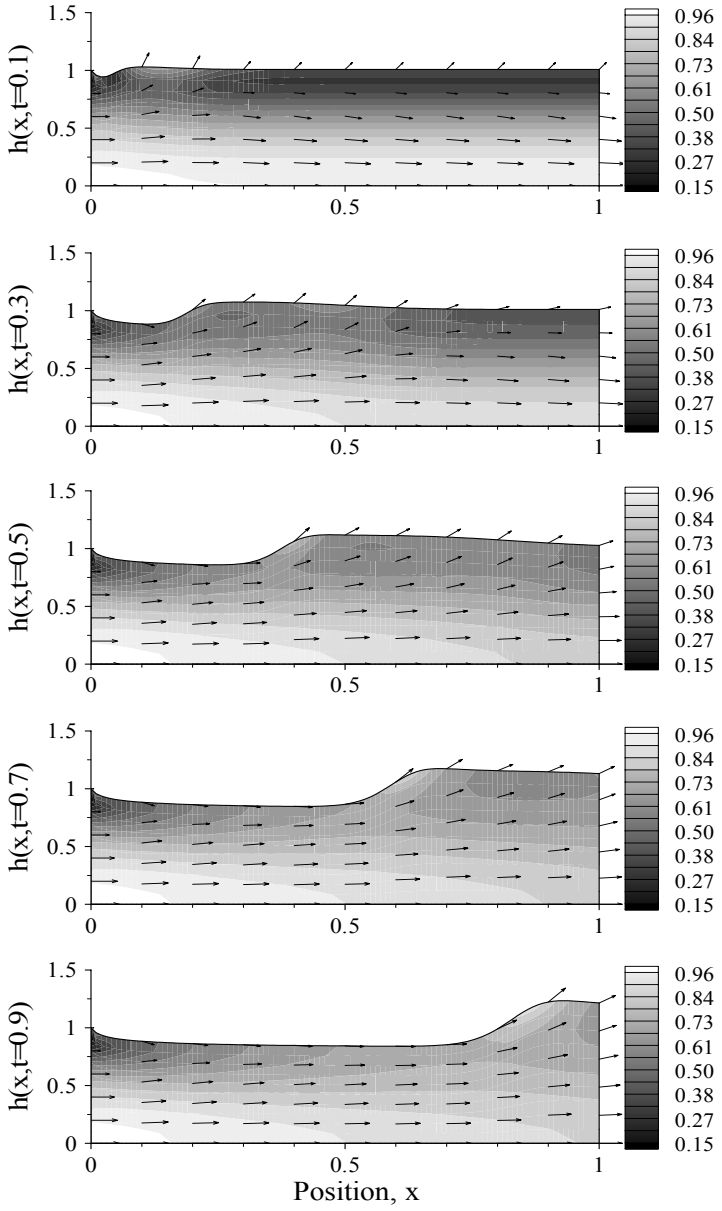

Fig. 11 Evolution of flow field and contours of velocity magnitude for moderately low-inertia flow, Re = 10, in the absence of gravity. The figure shows the flow fields at constant intervals 0.2 over a period of 0.9 time units.

velocity component at the free surface is shown in Fig. 8b at the same intervals of time. The velocity increases from zero at the channel exit, and reaches a maximum, which weakens with time. It then decreases and levels off further downstream. With time, the free surface velocity increases gradually, eventually reaching the steady-state solution, this latter being an envelope to the transient solution. Further insight is gained by examining the depthwise velocity component at the free surface w(x, z = h, t) shown in Fig. 8c. The depthwise velocity undergoes a sudden drop corresponding to the sharp drop in the film thickness as the fluid emerges from the channel. It then experiences a maximum, coinciding with the crest of the film height. It is interesting to note that while the amplitude of the film height increases with time that of w tends to remain unchanged. Further downstream the depthwise velocity attains a constant value, which after some time becomes essentially zero. This behavior is simultaneously reflected in the stagnation

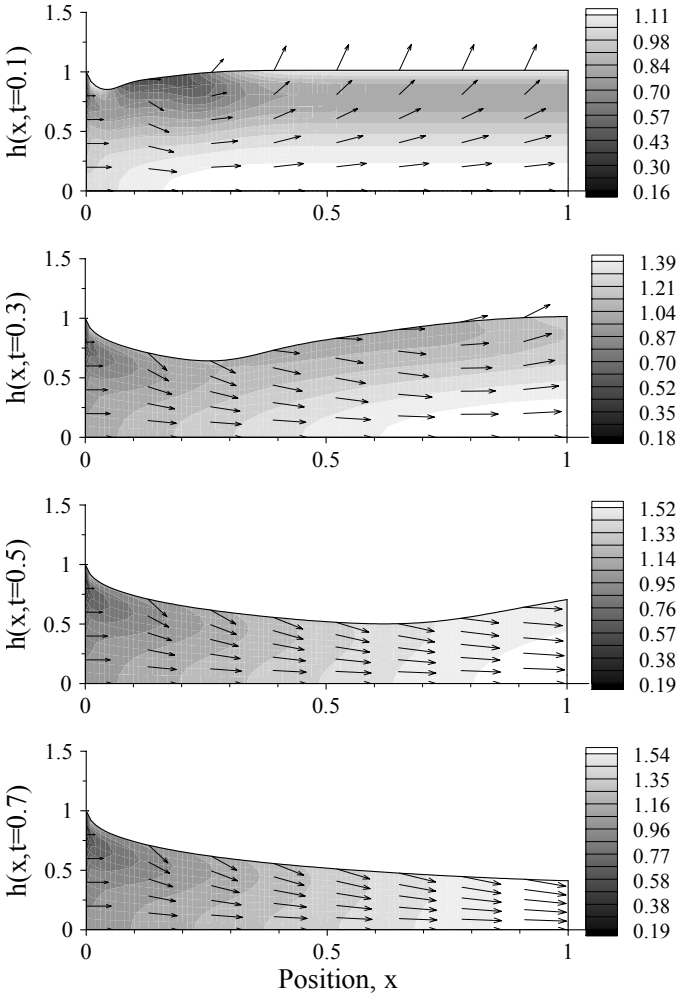

Fig. 13 Evolution of flow field and contours of velocity magnitude for moderately low-inertia flow, Re = 10, in the presence of strong influence of gravity, Fr = 1. The figure shows the flow fields at constant intervals 0.2 over a period of 0.7 time units.

of the film height ahead of the wave (see Fig. 8a). Figure 9 shows the flow fields at the same time intervals as in Fig. 8. It is evident from the figure that the initial similarity (parabolic) flow is quickly replaced by an almost uniform flow downstream of the disturbance in the early stage. In this region, the initial shearing has considerably diminished, leaving only a 40% difference in flow strength (velocity magnitude) between the free-surface and core regions. This is of course expected since viscous effects are dominant for this flow. With time, however, the regions ahead and behind the disturbance wave evolve into plug-flow regions, leaving most of the flow activity concentrated at the level of the disturbance. In fact, the flow remains strong in the whole region below the wave crest, and is typically 5 to 6 times stronger than elsewhere in the film.

There is a dramatic departure in flow behavior when the level of inertia is increased. The flow response at moderately low inertia (Re = 10) is depicted in Figs. 10 and 11. As shown in Fig. 10a, although the initial jump (formation of a sine wave) in film surface near the channel exit is similar to that in the case of low-inertia flow (compare with Fig. 8a), the wave tends to evolve into a hydraulic-jump like structure than the symmetric wave predicted for Re = 1. It is apparent from the figure that the wave front broadens with increase in Reynolds number. There is also an increase in the time required to reach the steady state (30% longer between Re = 1 and 10). It is interesting to observe that the streamwise velocity profile retains essentially the same shape regardless of the Re value (compare Figs. 8b and 10b). In contrast, the depthwise velocity experiences a total loss of symmetry, with significant (one order of magnitude) loss of amplitude, weakening of the maximum, and the emergence of additional extrema. The formation of the hydraulic-jump structure is clearly evident upon examining the evolution of the flow field at different time levels as shown in Fig. 11. The flow in the majority of the film region tends to remain parabolic as imposed initially for a much longer period of time than at low Reynolds number. It is only after the passage of the disturbance wave that the flow loses its similarity (parabolicity). In contrast to the situation in Fig. 9, the flow at the wave jump is only slightly stronger than elsewhere in the film.

The influence of gravity on transient behavior of the flow is shown in Figs. 12 and 13. In this case, Fr = 1 and Re = 10. It is clear from the figure that gravity tends to prohibit the formation of a soliton-like wave. Instead, a depression disturbance forms, reflecting a strong contraction that emanates at the channel exit (Fig. 12a). The depression grows with time, leading eventually to a contraction over the whole jet domain (when steady state is attained). Gravity thus acts like a drawing force, enhancing elongational flow as deciphered from Fig. 12b, which in turn leads to the strengthening of the depthwise flow toward the jet axis (Fig. 12c). The time that is needed for the steady state to be obtained over the whole computational domain is only 0.7 of a time unit. Figure 13 shows the evolution of the flow field at different time levels over a period of 0.7 of a time unit. The strength of the vertical flow is particularly obvious at t = 0.1, which is downward near the exit and upward further downstream. Although the flow strengthens with time, it tends to align itself with the free surface. The depression near the channel exit clearly impacts the flow everywhere as it propagates downstream with time. The flow essentially evolves from a semi-parabolic dependence with height to one experiencing a minimum below the free surface (see in particular Fig. 13 for t = 0.7).

The influence of the initial conditions is now examined by considering exponentially decreasing profiles for the initial film thickness and velocity. These initial conditions simulate a practical situation, where the initial state of the fluid corresponds to a fluid film with a thickness that decreases with x. The velocity distribution is also assumed to decrease with x, but follows the parabolic dependence on z similar to the velocity distribution inside the channel, and diminishing downstream from the exit. Exponential decrease of velocity along the x direction is taken to simulate a stationary liquid. These conditions may be realized experimentally by assuming a film that is being extruded from a channel and drawn at some distance downstream. If the process is suddenly stopped and the drawing mechanism is removed, the conditions at which extrusion of the fluid starts again are very similar to the initial conditions assumed here. It would be ideal to set the velocity equal to zero in the whole computational domain; however this is not possible since the continuity between initial and boundary conditions must be satisfied. Thus, it is assumed that

$$f(x) = g(x) = e^{-3x}. \qquad (21)$$

Gravity is assumed to be negligible. Figure 14 shows the evolution of the free surface at time t = 0.1, 0.3, and 0.5 for Re = 1. Initial free surface and steady-state are shown by dashed and dotted line, respectively. The figure indicates that the growth rate of the wave for decreasing initial conditions is faster than for flat initial conditions (see Fig. 8). The rapid growth in the amplitude causes steepening of the front and tail of the wave. Although the amplitude grows considerably at this low Reynolds number, shock formation is not observed. There

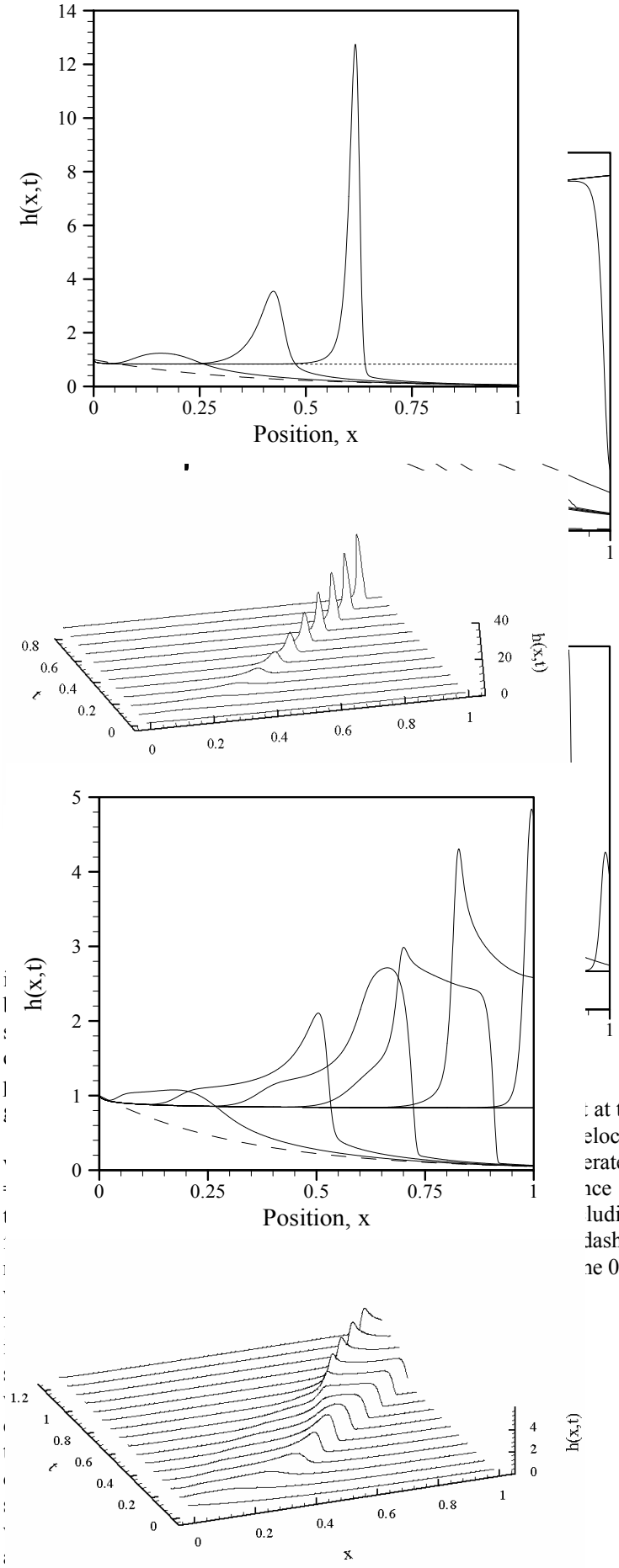

Fig. 15 Evolution of free surface for moderately low-inertia flow, Re = 10, in the absence of gravity, at constant intervals 0.2, including exponentially decreasing initial profile (dashed line), and three-dimensional perspective.

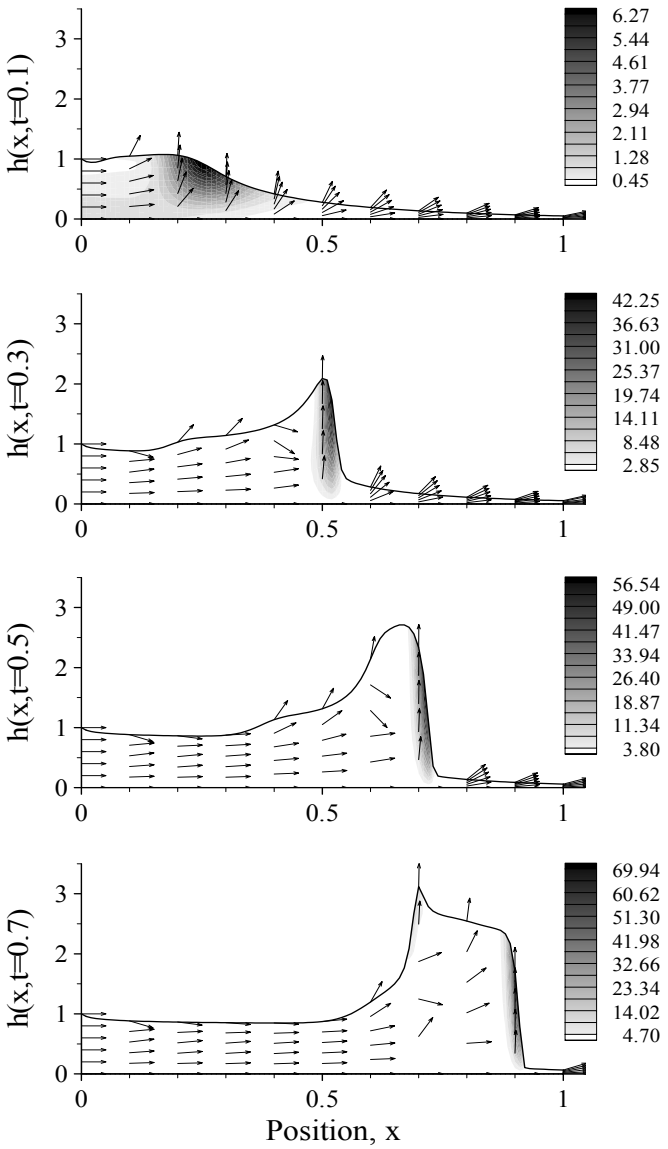

Fig. 17 Evolution of flow field and contours of velocity magnitude for moderately low-inertia flow, Re = 10, in the absence of gravity at constant intervals 0.2. Vector length is unit.

negligible value. The drop in u leads to significant elongational effect, which in turn causes a strong depthwise flow as depicted in Fig. 16b. In the early stages, w displays only one maximum, which coincides with the crest of the film wave. The steepening of the wave at both the tail and front is accompanied by the formation of two maxima in w, which are evident from the inset in Fig. 16b, corresponding to the fourth wave in Fig. 15. Details of the flow field are further given in Fig. 17, including the flow strength and direction at various stages. In the early stage, the flow strength is relatively evenly distributed throughout the film ($t < 0.1$). However, considerable flow activity develops in the front region, at later stages, leaving the flow under relative stagnant conditions upstream of the wave. Elongational effects are clearly significant in this case.

Several distinct changes in flow response occur when

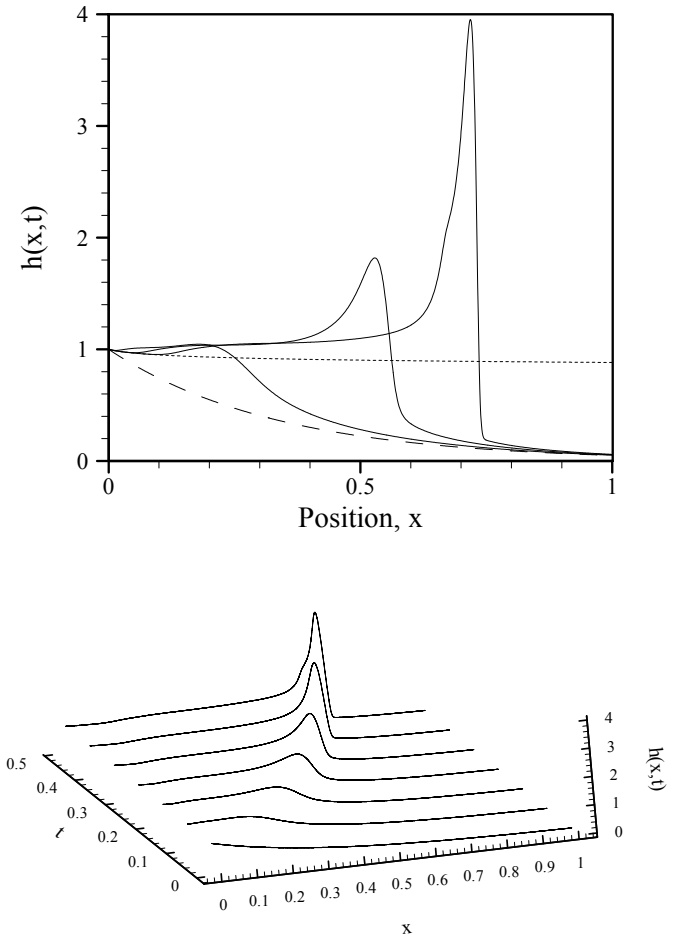

Fig. 18 Evolution of free surface for high-inertia flow, Re = 100, in the absence of gravity, at time t = 0.1, 0.3, and 0.5, including exponentially decreasing initial profile (dashed line), steady-state profile (dotted line), and three-dimensional perspective.

Reynolds number is further increased. For Re = 100, Fig. 18 shows that the wave experiences lengthening of the tail in time (compare with Figs. 14 and 15 for Re = 1 and 10). The flow recovers some simplicity similar to the low inertia flow (Fig. 14), after exhibiting wave of complex shape for Re = 10 (Fig. 15). The steepening is mainly observed at the front of the wave. The shock forms at $t \approx 0.5$, leaving no possibility for further development (broadening) of the wave.

It is important to note that the current results are not expected to be accurate in the presence of sharp flow gradient or severe curvature in the film surface; this would violate the basic assumption for boundary-layer flow. What can be drawn

from the present results are trends that one may expect to observe in reality under flow conditions similar to those investigated here. Only comparison with the fully two-dimensional solution will give a better quantitative estimate of the present inaccuracies.

CONCLUSION

The two-dimensional Newtonian jet of a thin fluid film emerging from a channel is examined in detail in this study. The influence of inertia and gravity is investigated. The thin-film equations are solved by expanding the flow field in orthonormal modes over the depth. The Galerkin projection method is applied to generate the equations that govern the expansion coefficients. The method predicts the shape of the free surface, the flow field as well as the force within the film. Most results reported are based on the first four-mode solution, since higher-order modes are shown to have an insignificant influence on the solution. It is found for fluids with any Reynolds number that the thickness of the jet contracts until it reaches its final value at some distance from the exit. When gravity is relatively strong, a considerable thinning of the film is predicted. The depthwise flow component is even stronger in this case. The film may or may not develop a shock, depending on the flow parameters and initial conditions. It is found, for instance, that if the initial film thickness is streamwise decreasing, the film tends to form a wave that propagates downstream in time with continuous steepening. This steepening, after some time, results in the shock-like structure. The rapid transient nonlinear behavior suggests the existence of a wide range of geometrical and flow parameters under which steady state cannot be achieved.

NOMENCLATURE

Fr	Froude number
g	gravitational acceleration
h	dimensionless jet thickness
H	jet thickness at x = 0
L	characteristic length
M	number of modes
Re	Reynolds number
t	time
u	streamwise velocity component
U	expansion coefficient
V	maximum velocity inside the channel
w	depthwise velocity component
x	streamwise coordinate
z	depthwise coordinate
ε	aspect ratio
Φ	basis function
χ, ξ	transformed coordinates
τ	transformed time
δ_{ij}	Kronecker delta
ρ	density
μ	viscosity
Ω	domain occupied by fluid

ACKNOWLEDGMENTS

This work was supported by the Natural Science and Engineering Research Council of Canada.

REFERENCES

1. J. R. A. Pearson, *Mechanics of Polymer Processing* (Elsevier Applied Sciences, New York, 1985)
2. S. Middleman, *Fundamentals of Polymer Processing* (McGraw-Hill, New York, 1977)
3. D. B. Harmon, Drop size from low speed jets, *J. Franklin Inst.* **259**, 519 (1955)
4. J. P. K. Tillett, On the laminar flow in a free jet of liquid at high Reynolds numbers, *J. Fluid Mech.* **32**, 273 (1968)
5. K. Addachi, Laminar jets of a plane liquid sheet falling vertically in the atmosphere, *J. Non-Newtonian Fluid Mech.* **24**, 11 (1987)
6. S. L. Goren and S. Wronski, The shape of low-speed capillary jets of Newtonian liquids, *J. Fluid Mech.* **25**, 185 (1966)
7. S. Middleman, Modeling Axisymmetric Flows. Dynamics of Films, Jets, and Drops (Academic Press, San Diego, 1995)
8. R. E. Nickell, R. I. Tanner and B. Caswell, The solution of viscous incompressible jet and free surface flows using finite-element methods, *J. Fluid Mech.* **65**, 189 (1974)
9. K. R. Reddy and R. I. Tanner, Finite element solution of viscous jet flows with surface tension, *Computers and Fluids* **6**, 83 (1978a)
10. B. J. Omodei, Computer solutions of a plane Newtonian jet with surface tension, *Computers and Fluids* **7**, 79 (1979)
11. R. I. Tanner, *Engineering Rheology*, 2nd ed., (Oxford University Press, New York, 2002)
12. S. Middleman and J. Gavis, Expansion and contraction of capillary jets of Newtonian liquids, *Phys. Fluids* **4**, 355. Errata: *Phys. Fluids* **4**, 1450
13. H. C. Chang, Wave evolution on a falling film. *Annu. Rev. Fluid Mech.* **26**, 103 (1994)
14. A. Oron, S. H. Davis, and S. G. Bankoff, Long-scale evolution of thin liquid films. *Rev. Mod. Phys.* **69**, 931 (1997)
15. S. V. Alekseenko, V. E. Nakoryakov, and B. G. Pokusaev, Wave formation on a vertical falling liquid film, *AIChE J.* **31**, 1446 (1985)
16. T. Prokopiou, M. Cheng, and H.-C. Chang, Long waves on inclined films at high Reynolds number, *J. Fluid Mech.* **222**, 665 (1991)
17. E. J. Watson, The radial spread of a liquid jet over a horizontal plane, *J. Fluid Mech.* **20**, 481 (1964)

18. A. Z. Szeri, Some extensions of the lubrication theory of Osborne Reynolds, *Trans. ASME J. Tribol.* **109**, 21 (1987)
19. D. Quere, Fluid coating on a fiber, *Ann. Rev. Fluid Mech.* **31**, 347 (1999)
20. O. Takeshi, Surface equation of falling film flows with moderate Reynolds number and large but finite Weber number, *Phys. Fluids* **11**, 3247 (1999)
21. R. E. Khayat and S. Welke, Influence of inertia, gravity and substrate topography on the two-dimensional transient coating flow of a thing Newtonian fluid film. *Phys. Fluids* **13**, 355 (2001)
22. M. R. Siddique and R. E. Khayat, Influence of inertia and topography in thin-cavity flow. *Phys. Fluids* **14**, 1703 (2002)
23. R. E. Khayat, Influence of inertia on the transient axisymmetric free-surface flow inside thin cavities of arbitrary shape, *Phys. Fluids* **13**, 3636 (2001)
24. K. Kim and R. E. Khayat, Transient coating flow of a thin non-Newtonian fluid film, *Phys. Fluids* **14**, 2202 (2002)
25. R. E. Khayat, Transient two-dimensional coating flow of a viscoelastic fluid film on a substrate of arbitrary shape, *J. Non-Newtonian Fluid Mech.* **95**, 199 (2000)
26. B. J. Hamrock, *Fundamentals of Fluid Film Lubrication.* (McGraw-Hill, New York 1994)
27. D. J. Benney, Long waves in liquid films, *J. Math. Phys.* **45**, 150 (1966)
28. T. R. Salamon, R. C. Armstrong, and R. A. Brown, Travelling waves on vertical films: Numerical analysis using the finite-element method, *Phys. Fluids* **6**, 2202 (1994)
29. V. Y. Shkadov, Wave condition of a flow in a thin viscous layer under the action of gravitational forces, *Izv. Akad. Nauk SSSR Mekh. Zhidk. Gaza* **1**, 43 (1967)
30. J. R. Bertschy, R. W. Chin and F. H. Abernathy, High-strain-rate free-surface boundary-layer flows, *J. Fluid Mech.* **126**, 443 (1983)
31. C. Ruyer-Quil, P. Manneville, Modeling film flows down inclined planes, *Eur. Phys. J. B* **6**, 277 (1998)
32. J.-J. Lee and C. C. Mei, Stationary waves on an inclined sheet of viscous fluid at high Reynolds and moderate Weber numbers, *J. Fluid Mech.* **307**, 191 (1996)
33. O. C. Zienkiewicz and J. C. Heinrich, A unified treatment of steady-state shallow water and two-dimensional Navier-Stokes equations—finite-element penalty function approach, *Comp. Meth. App. Mech. Eng.* **17/18**, 673 (1979)
34. G. R. Sell, C. Foias, and R. Temam, *Turbulence in Fluid Flows : A Dynamical Systems Approach*. (Springer-Verlag, New York, 1993)
35. A. E. Deane, I. G. Kevrekidis, G. E. Karniadakis and S. A. Orszag. Low-dimensional models for complex geometry flows: Application to grooved channels and circular cylinders. *Phys. Fluids A* **3**, 2337 (1991)
36. P. Holmes, J. L. Lumley, and G. Berkooz, *Turbulence, Coherent Structures, Dynamical Systems and Symmetry* (Cambridge University Press, Cambridge, 1996)
37. R. E. Khayat and N. Ashrafi, A low-dimensional approach to nonlinear plane-Poiseuille flow of viscoelastic fluids, *Phys. Fluids* **14**, 1757 (2002)
38. R. E. Khayat, Transient free-surface flow inside thin cavities of viscoelastic fluids *J. Non-Newtonian Fluid Mech.* **91**, 15 (2000)